Document downloaded from:

http://hdl.handle.net/10251/94882

This paper must be cited as:

Landi, SJ.; Carneiro, J.; Fernandes, F.; Parpot, P.; Molina Puerto, J.; F. Cases; Fernández Sáez, J.... (2017). Functionalization of Cotton by RGO/TiO2 to Enhance Photodegradation of Rhodamine B Under Simulated Solar Irradiation. Water Air & Soil Pollution. 228(335). doi:10.1007/s11270-017-3533-z

The final publication is available at

https://doi.org/10.1007/s11270-017-3533-z

Copyright Springer-Verlag

Additional Information

Functionalization of Cotton by RGO/TiO2 to Enhance Photodegradation of Rhodamine B Under Simulated SolarIrradiation

S. Landi Jr[1,3], , J. O. Carneiro[1,2*], F. Fernandes[1], P. Parpot[4], , J. Molina[5], F. Cases[5], J. Fernández[5], J. G. Santos[6], G. M. B. Soares[6], V. Teixeira[1], A. P. Samantilleke[1,*]

[1]*Center/Department of Physics, University of Minho, Campus of Azurém, 4800-058, Guimarães, Portugal*

[2]*Instituto Superior Politécnico de Tecnologias e Ciências, Av. Luanda Sul, Rua Lateral Via S10, Talatona – Município de Belas Luanda / Angola*

[3] *Instituto Federal Goiano, 75901-970, Rio Verde, Goiás, Brazil*

[5]*Departamento de Ingeniería Textil y Papelera, EPS de Alcoy, Universitat Politècnica de València, Plaza Ferrándiz y Carbonell s/n, 03801 Alcoy, Spain*

[6]*Department of Textile, University of Minho, Campus of Azurém, 4800-058, Guimarães, Portugal*

Abstract

Keywords: Rhodamine B, reduced graphene oxide, titanium dioxide, photocatalysis.

* Corresponding author. A. P. Samantilleke

E-mail addresses: carneiro@fisica.uminho.pt (J. O. Carneiro), b6073@fisica.uminho.pt (F. Fernandes), salmon.landi@ifgoiano.edu.br (S. Landi Jr), anura@fisica.uminho.pt (A.Samantilleke), jamopue@doctor.upv.es (J. Molina), fjcases@txp.upv.es (F. Cases), marianapastor88@gmail.com (M. Pastor), jsantos@det.uminho.pt (J.Santos), gmbs@det.uminho.pt (G.Soares), davideamsilva@gmail.com (D.Silva), E.A.Luís, A.A.Chivanga Barros, vasco@fisica.uminho.pt (V. Teixeira).

Abstract

Reduced graphene oxide (RGO) and nanoparticles of TiO_2 were immobilized on cotton textile substrates to produce self-cleaning textiles. The XRD and Zeta potential measurements of starting materials were crucial for innovative methods of functionalization. Different number of RGO and TiO_2 coatings were applied, 1-3 and 1-2, respectively. In this context, photocatalytic degradation of Rhodamine B (Rh-B) solution was carried out in a photoreactor thereby allowing a laminar flow by irradiation with light simulated sunlight. SEM, UV-vis reflectance diffuse spectra and severe washing showed the good adhesion of the RGO and TiO_2 nanoparticles on the samples

It can be observed that the application of different number of RGO andTiO_2 coatings has influence on photocatalytic properties of functionalized cotton textile substrates. All five de-ethylated intermediates of Rh-B during the photocatalytic degradation were identified by an HPLC method. The experimental results show that, in general, the higher the number of RGO coatings the higher the photocatalytic efficiency of the functionalized substrate is. Moreover, the increased number of RGO coatings seems to have more influence in increasing photocatalytic efficiency than the corresponding increase of the number of TiO_2 coatings.

1 Introduction

TiO_2 powder is white in colour and therefore has no absorption in the visible region of electromagnetic spectra. In the last century, many studies were carried out with this semiconductor about its ability to produce certain chemical reactions under UV light irradiation [1]. In recent years, several studies aims at improving photocatalytic property of TiO_2 nanostructures by controlling their size, morphology, degree of crystallization,

as well as by doping with others materials have been reported [2]. Many reports in the field of TiO_2 photocatalysis investigated the degradation of pollutants such as pesticides [3], dyes [4] and pharmaceuticals [5] using the energy from the sun. In all the studies, two principal challenges have been identified namely, reducing recombination rate of photogenerated electron-hole pairs, because they are responsible for redox reactions which cause the degradation of organic pollutants and narrowing the wide bandgap of TiO2, since only ~5% of the solar flux that reaches the surface of the earth lies in the UV region. Despite these two fundamental issues, TiO_2 is used commonly mainly due to its abundant availability, low-cost, nontoxicity and high chemical stability. Furthermore, it can be deposited or mounted on rigid or flexible substrates, such as glass, fibres or stainless steel. [6]. In the past few decades, doping with metal ions [7], coupling with a second semiconductor [8], and anchoring TiO_2 particles onto a large-surface-area (silica [9,10], zeolites [11], carbon-based materials [12,13] and others [14]) have all been elucidated as efficient techniques to improve the quantum efficiency and the reaction rates for environmental decontamination under visible or UV light irradiation. Alternatively, graphene, in particular, has been regarded as an extremely attractive component for the preparation of composite materials [15]. In addition to its large theoretical specific surface area, graphene has an extensive two-dimensional π-π conjugation structure, which endows it with excellent conductivity of electrons. When combining TiO_2 nanocrystals with graphene, excited electrons will transfer from the conduction band of TiO_2 to graphene via a percolation mechanism. Here, graphene acts as an excellent electron-acceptor/transport material effectively facilitating the migration of photoinduced electrons and suppressing charge recombination [16].

In this work, we report surface modification of cotton textiles using different coatings of reduced graphene oxide and TiO_2 nanoparticles (RGO/TiO_2) by a facile method and evaluate their photocatalytic potential by measuring the degradation rate of Rhodamine B (Rh-B) in an aqueous solution under simulated sunlight irradiation.

2 Experimental

2.1 Materials and methods

TiO_2 nanoparticles (Aeroxide P25 TiO_2) purchased from Quimidroga (Spain) consisted of a mixture of the anatase (80%) and rutile (20%) crystalline phases. Graphene oxide powder was acquired from Nanoinnova Technologies S.L. (Spain) and sodium dithionite ($Na_2S_2O_4$) was acquired from Merck.

2.2 Surface Functionalization

2.2.1 Scouring

Before the functionalization process, the cotton substrates (12.5x12.5 cm) were scoured with 2 mgL^{-1} of a nonionic and anionic detergent (Kieralon OLB-New) during 1h at 70 ºC where, the solution to cotton textile weight ratio was 50:1. The samples were then rinsed with distilled water and finally dried at room temperature for 24 h.

2.2.2 Synthesis of reduced graphene oxide on cotton substrate

A 1 gL^{-1} graphene oxide (GO) solution was ultrasonicated for 1 h, following which, the cotton substrates were immersed in the GO solution for further1 h to allow the adsorption of GO sheets on the surface of the samples. After drying under ambient conditions the cotton substrates were placed in a solution containing the reducer agent

(50 mM $Na_2S_2O_4$) at 90º C for 30 min. Samples with a different number of RGO coatings (1-3) were obtained repeating the procedure mentioned above [8].

2.2.3 Functionalization of TiO_2 on the cotton-RGO

After the functionalization with RGO, the samples were immersed in a 4 gL^{-1} of TiO2 nanoparticles solution (pH=2–3) during 1 min. The cotton substrates were then pressed twice under 2,00 bar pressure with horizontal rollers (9,0 rpm). Finally, the prepared substrates were dried in an oven at 100 ºC for 10 min. Fig.1 shows a schematic representation of the functionalization procedure.

The cotton substrates are denoted in this work by CO-n_1RGO/n_2TiO_2, where n_1 and n_2 denote the number of the RGO and TiO_2 coatings, respectively and CO, the substrate of cotton. The number of the RGO coatings was varied between 1 and 3 and the TiO_2 was 1 or 2.

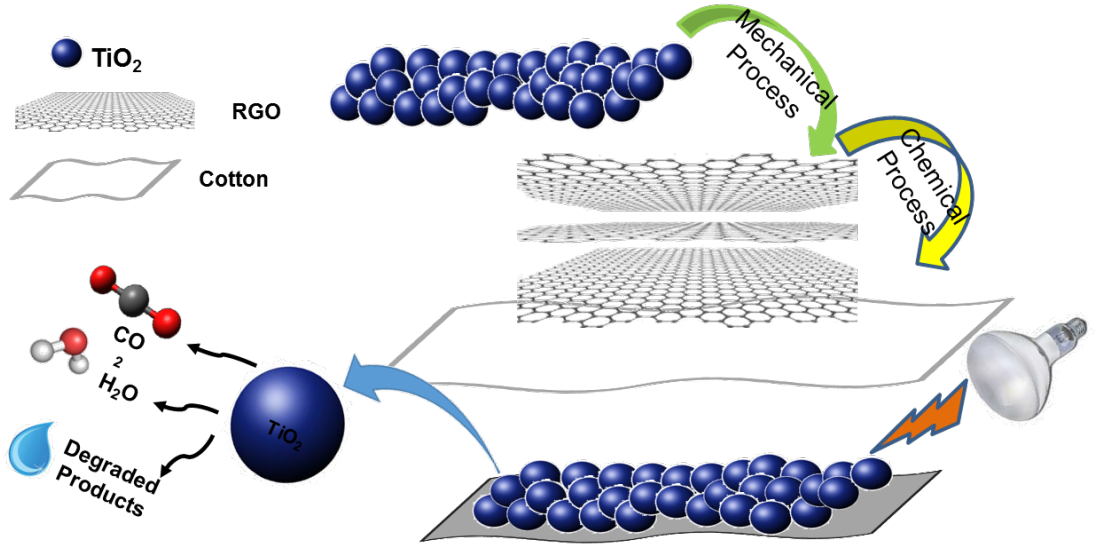

Fig. 1. **A schematic illustration of the functionalization Procedure**

2.3 X-ray diffraction (XRD)

The XRD patterns of TiO_2, GO and RGO powder were acquired in the range of 10º–70º (2θ) using a Bruker D8 Discover X-ray diffractometer with the conventional Bragg–Brentano geometry.

2.4 Zeta Potential measurements

The zeta-potential measurements were performed on a Zetasizer NS 2007 from Malvern Instruments, UK of the TiO_2, GO and RGO aqueous dispersions with corresponding pH range between 2 and 10.

2.5 FTIR analysis

Fourier transformed infrared (FTIR) spectra of GO, RGO and TiO_2 powders were obtained using Nicolet, Avatar-FTIR 360. Attenuated total reflectance (ATR) measurement mode was used with the sample 400 cm^{-1} to 4000 cm^{-1} wavenumber range.

2.6 UV-vis diffuse reflectance spectra (DRS)

UV–vis diffuse reflectance spectra (DRS) were obtained using a spectrophotometer ScanSpecUV-vis, ScanSci equipped with an integrating sphere assembly, using Barium Sulfate ($BaSO_4$) as the reference sample. The spectra were recorded at room temperature in air within the range of 300–700 nm. Spectra were obtained for the uncoated cotton and for all the functionalized samples.

2.7 Electrochemical impedance spectroscopy (EIS) measurements

An Autolab PGSTAT302 potentiostat/galvanostat was used to perform EIS measurements in the 10^5-10^{-2} Hz frequency range. The amplitude of the sinusoidal voltage used was ± 10 mV. Measurements were carried out in a two-electrode arrangement with two types of configuration:(a) The sample was located between two round copper electrodes (A = 1.33 cm^2) to measure the bulk resistance. (b) Two rectangular copper electrodes (0.5 cm×1.5 cm) separated by 1.5 cm pressing on the fabric sample. The measured area of the fabric with this configuration was a square of 1.5 cm, so the measured impedance modulus (Ω) was equal to the surface resistivity (Ω/□).

2.8 Electrochemical impedance spectroscopy (EIS) measurements in solution

A standard three-electrode design was employed to measure the EIS response of CO-RGO samples in 0.1 M H_2SO_4 solutions. An asymmetrical configuration metal/sample/electrolyte was employed. Samples were mounted on a stainless steel plate (employed to produce the electrical connection). An Ag/AgCl (3.5 M KCl) electrode and stainless steel rod were employed as reference electrode and counter electrode, respectively. The effective area of the samples exposed to solution was 0.28 cm^2.The experimental results were also fitted using a non-linear least squares fitting minimization method by ZView software (version 2.7).

2.9 Scanning electrochemical microscopy (SECM)

SECM measurements were carried out with a scanning electrochemical microscope of Sensolytics. A three-electrode configuration cell consisting of a 100-μm-diameter Pt microelectrode, a Pt wire auxiliary electrode and Ag/AgCl (3.5 M KCl) reference electrode. The cotton were not polarized and the experiments were performed at their

open circuit potential. Measurements were performed in $K_4Fe(CN)_6$0.01 M and 0.1 M KCl (supporting electrolyte). The potential of the microelectrode was fixed at +0.4 V, potential at which the reduced form of the redox mediator is oxidized at its diffusion limit. All the experiments were carried out in inert nitrogen atmosphere. The substrates were samples (0.5 x 0.5 cm^2) cut from the cotton and glued on glass microscope slides with epoxy resin. Approach curves were employed to test the electroactivity of the samples and the approach rate employedwas 10 $\mu m \cdot s^{-1}$.

In the experiments with irradiation, ultraviolet light was applied with a ThermoOriel 66901 Universal Lamp Housing (mercury lamp 50/500 W) operating at 300 W. Light was conducted to the SECM with optical fiber. Measurements with UV light were performed with the microelectrode at a constant height of 50 μm above the sample. The variation of the oxidation current at +0.4 V with time andpulses of irradiation applied was registered.

2.10 Photocatalytic measurements

The photocatalytic activity of all samples was evaluated by measuring the degradation rates of Rh-B aqueous solutions (4 mgL^{-1}) under similar radiation sunlight. Rh-B (an important xanthene cationic dye) was selected because of its well-defined optical absorption characteristics and good resistance to light degradation. Moreover, this organic dye is one of the most common pollutants present in the effluents from textile industries in developed countries.

In a typical experiment, the CO-RGO/TiO_2 samples were dipped into a photocatalytic reactor (Fig.2) with 400 mL of Rh-B aqueous solution. The system was stirred for 20 min in the dark to reach the adsorption–desorption. The samples were irradiated with a 300 W lamp (ULTRA-VITALUX 300W E27) placed at a distance around 20 cm above

the sample's surface. The average irradiance was around 40 W/m^2 (measured with a UV light Meter LTLutron YK-35UV).

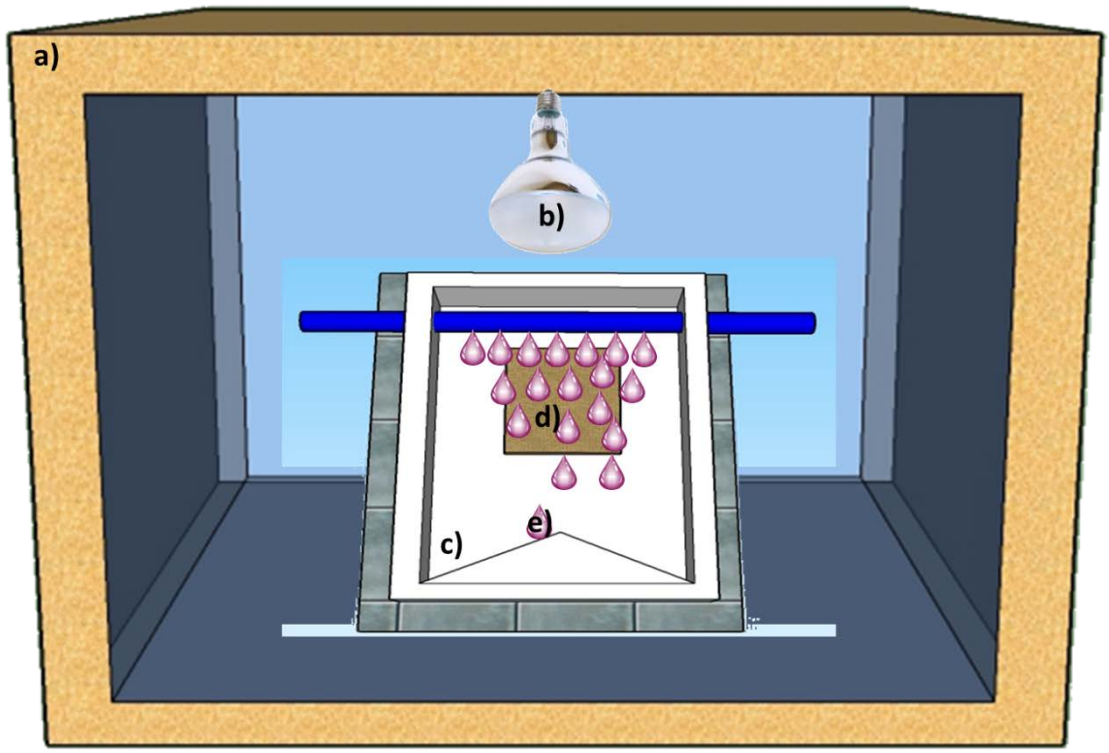

Fig. 2. Schematic diagram of the experimental setup: (a) light system, (b) UV lamp reservoir, (c) photoreactor, (d) catalyst substrate and (e) solution of rhodamine B.

The absorbance of the Rh-B solution was monitored during 120 min, at time intervals of 20 min up to 40 minutes and then at intervals of 40 min up to 120 min, using a spectrophotometer (ScanSpecUV-vis, ScanSci) in the range of 300–700 nm. For this, some aliquots of Rh-B solution (3.5 mL) were taken out and then analyzed by monitoring the magnitude variation of its main absorption peak (around 554 nm). The rate of Rh-B consumed can be verified by ratio, that is called photocatalytic efficiency (η):

$$\eta = (C_0 - C)/C_0, \quad (1)$$

where C is the concentration of Rh-B solution after similar sunlight irradiation and C_0 is the initial concentration after circulating in dark for 20 min. At low concentrations, the absorbance of the solution (measured quantity) is related to the solution's concentration through the Beer–Lambert law, that is, $A=\varepsilon.l.C$, where ε is the molar extinction coefficient and l is the light path length. Therefore, $A/A_0=C/C_0$ and then:

$$\eta = 1 - A/A_0. \quad (2)$$

Consequently, the change of Rh-B concentration can be evaluated by measuring the change in the intensity of its main absorption peak.

2.11 Washing process

In order to evaluate the degree of adsorption of RGO and TiO_2 on the cotton substrates, several washes were performed after the degradation photocatalytic essays. In this process

the samples were subjected to five washes (60 °C) in an "up and down" machine (FE Lupton Lta, England). Each sample was placed in a tube with the washing solution that was made with distilled water and detergent (ECE). Each wash lasted 20 minutes and between washes the washing solution was renewed. After performing this procedure, the cotton substrates were subjected again to the Rh-B degradation photocatalytic essays and was determinate their new photocatalytic efficiencies.

2.12 Scanning electron microscope (SEM)

The morphology and elemental composition of all samples were examined by scanning electron microscopy (SEM, NanoSEMFEI Nova 200) and energy dispersive X-ray (0 – 10 kV), respectively.

2.13 HPLC analyses

The de-ethylation intermediates of Rh-B during the photocatalytic degradation were identified by HPLC-MS. The HPLC set-up consisted of a Thermo Finnigan Lxq equipped with a UV-visible diode array detector in series with a mass detector and a C-18 reverse-phase column (2.6 μm, 100 mm x 2.1 mm i.d., Kinetex®). Acetic acid solution (0.1%, v/v) and methanol were used as mobile phase at a flow rate of 0.4 mL/min. The gradient elution was carried out as follows: methanol percentage linearly increased form 40% to 80% during 15 min, then maintained at 80% for 10 min and finally decreased to the initial value during the last 5 min.

3. Results and Discussion

3.1 Structural characterization (XRD)

The XRD was employed to investigate the crystal structure of TiO_2 nanoparticles (and crystallite size), graphene oxide (GO) and reduced graphene oxide (RGO). X-ray diffraction patterns were obtained for TiO_2 powders (Fig. 3). Since TiO_2 powders were a mixture of anatase and rutile, different peaks can be observed in the XRD pattern. For this sample, the existence of both anatase and rutile phases can be identified by JCPDS file no. 21–1272 and no. 21–1276, respectively. The crystalline phases can be confirmed by the presence of (101), (004) and (200) diffraction peaks, in the case of anatase phase; and (110), (111) and (002) diffraction peaks for the rutile crystalline phase. Using the Debye–Scherrer equation, it was observed that the mean crystallite grain size of the TiO_2 particles was around 23 nm and 28 nm for anatase and rutile phases, respectively. These values were calculated from the full width at the half-maximum intensity of the (101) anatase diffraction peak (corresponding to $2\theta = 25.3^{o}$) and rutile diffraction peak (corresponding to $2\theta = 54.1^{o}$).

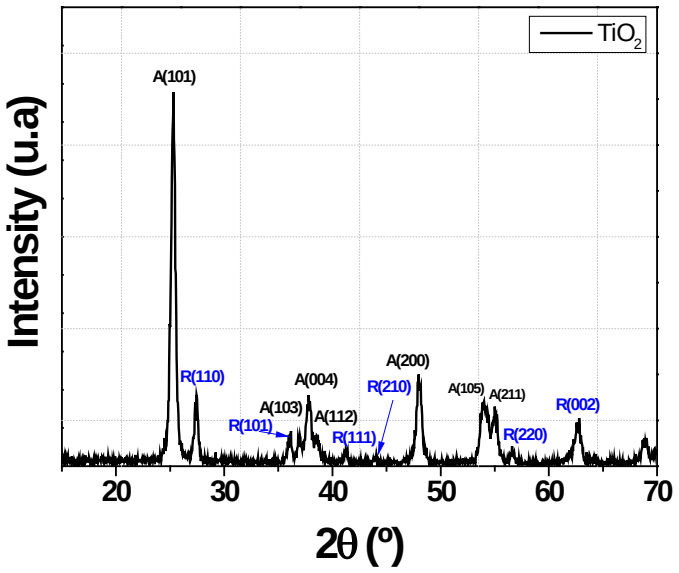

Fig. 3. XRD patterns of TiO_2 nanoparticles.

Fig. 4 shows XRD patterns of GO and RGO powders. The characteristic diffraction peak (002) of GO (corresponding to a lattice spacing of 0.749nm) is ascribed to the introduction of oxygenated functional groups, such as epoxy, hydroxyl (–OH), carboxyl (–COOH) and carbonyl (–C=O) groups attached on both sides and edges of carbon sheets. These surface functional groups will subsequently act as anchoring sites for metal complexes. The diffraction peak at around 43° is associated with the (100) plane of the hexagonal structure of carbon [16] . A single crystal X-ray diffraction study of the recrystatlized form of anhydrous sodium dithionite reveals an anion with C_2 geometry and a 16º O-S-S-O torsional angle; nearly eclipsed. (Crystal Data for recrystallized $Na_2S_20_4$ are a=6.539 (1) Å, b = 6.552(1) Å, c = 6.578(1) Å, V = 240.0(1) Å, β = 121.61 (1)º, space group = P2/c, Z = 2) [17]

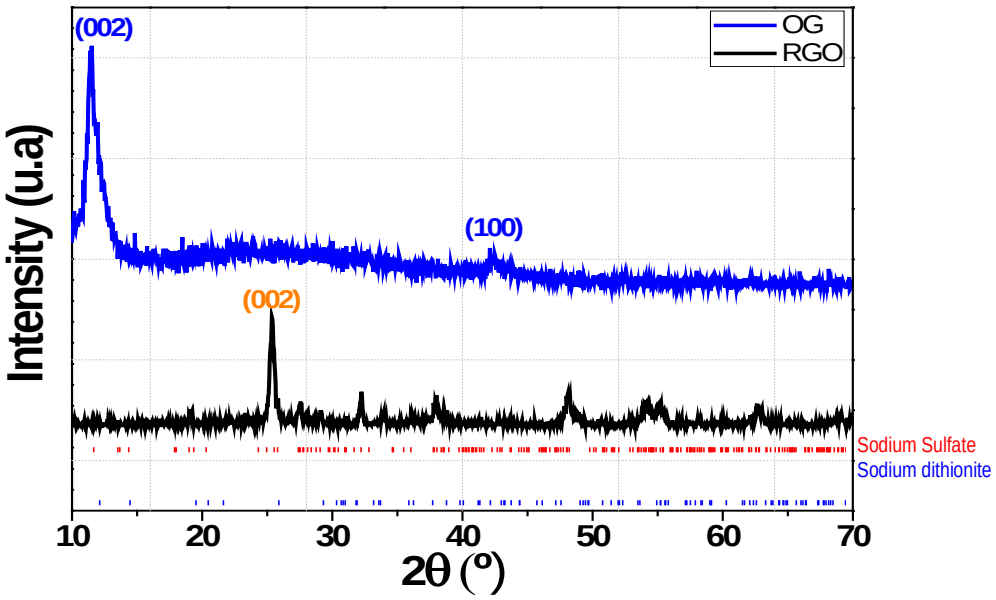

Fig. 4. XRD patterns of GO and RGO powders.

3.2 Electrokinetic behavior of TiO_2, GO and RGO powders

The zeta potential (ζ) is an important factor for characterizing the stability of colloidal dispersions. It is a measure of the negative charge around the double coating associated with the colloidal particle as a consequence of the ionization of different functional groups. Generally, particles with zeta potential in the range −30 mV to +30 mV are considered stable due to electrostatic repulsion [20].

The ζ curve for the TiO_2 nanoparticles is shown in Fig. 5. Anatase and rutile have identical chemical composition but different crystal systems and thus, their isoelectric point (IEP) occur at different pH values, 4.7 versus 6.2. The isoelectric pH value was found to be ~ pH 5.2. This is an acceptable value since it reflects the effect of the mixture of two the crystalline phases.

From Fig. 5 it is possible to observe that for pH < 5 the TiO_2 particles present positive ζ values that evidences the positive nature of its surface electrical charges, which also

contributes for the TiO_2 suspension stability via the appearance of repulsive electrostatic forces (Coulomb forces) [21].

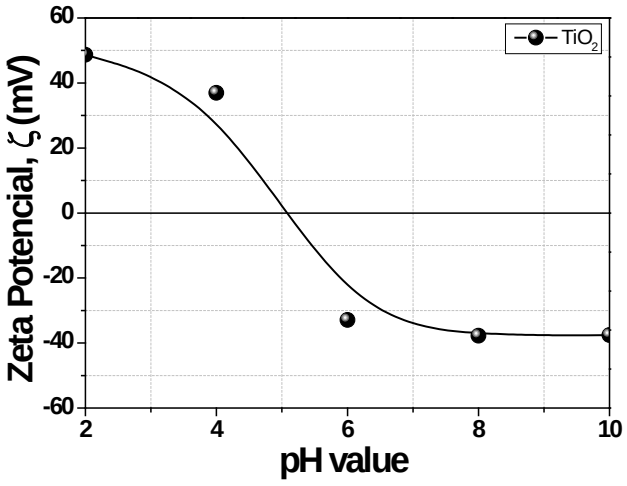

Fig. 5. Zeta-potential curve versus pH for the TiO_2 powders.

The measurements show that zeta potential for the GO colloids is pH sensitive, and effective dispersion of the colloids occurred within the pH range of 2–10 (Fig. 6). Experimentally, we observed that and the highest magnitude of ζ is obtained at pH 4 (−31.61 mV), although the pH range of 2–10 showed always (negative) charge [20].

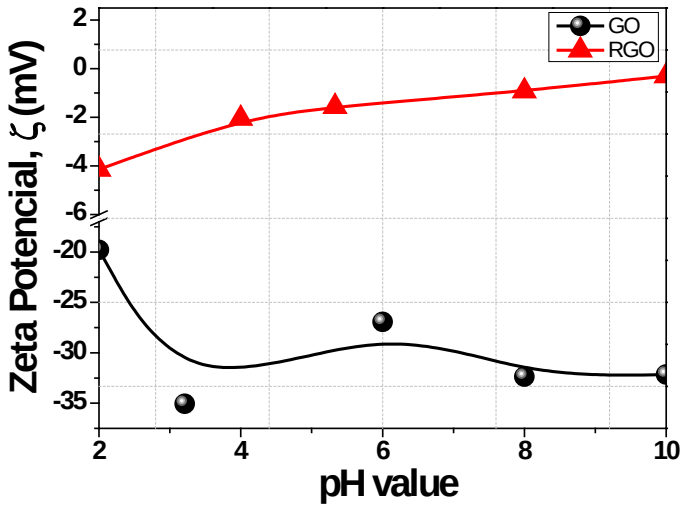

Fig. 6. Zeta potential of GO and RGO colloids at different pH.

The Figs 5 and 6 explain the strategy adopted for the functionalization: coated with RGO and then add TiO_2 nanoparticles from a solution with a pH <5.2. In these conditions, the assembly of the TiO_2 nanoparticles on the RGO coatings is possible due to the Coulomb forces. The nanoparticles are then retained due to the functional groups RGO's surface.

3.3 FTIR analysis

The FTIR spectrum in Fig. 7 in supplementary data showed the pure graphite spectrum shows an O–H stretching vibration band near 3436 cm^{-1} [22]. The peaks at 2928 and 2859 cm^{-1} indicate the asymmetric and symmetric vibrations of CH_2 groups, respectively. The peak at 1634 cm^{-1} is attributed to a C=C bond in pure graphite as well as in graphene. The absorption at 1110 cm^{-1}, which is the stretching type of vibrations of C–O bonds and 617 cm^{-1} (COO– wagging) are observed in the IR spectrum [22,23]. In the spectrum c), two absorption bands peaking at 3400 cm^{-1} and 1630 cm^{-1} , which are characteristic of O–H bending modes of adsorbed water and hydroxyl groups. Ti–O vibration occurs in the region of 400–800 cm^{-1} [23].

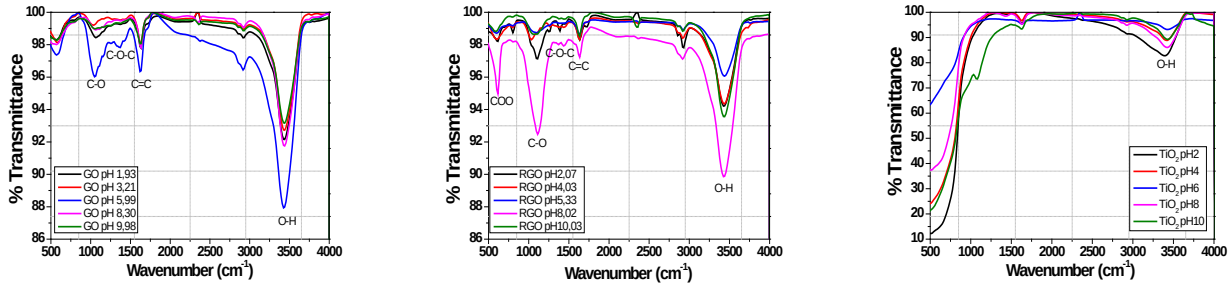

a) b) c)

Fig. 7. FTIR spectra of a) GO, b) RGO and c) TiO_2.

3.4 UV–vis diffuse reflectance spectra

It is important to characterize the light absorption of the cotton, since this will give us an indication of its absorption properties. Fig. 9 shows the diffuse reflectance spectra (DRS) for the different samples. Cotton showed the highest reflectance due to its white color. In general, TiO_2 coated samples showed a higher absorption in the UV region due to the presence of TiO_2 which presents its absorption in this region. Moreover, the addition of more RGO coatings induces the increase of absorbance in the UV region. After the reduction of graphene oxide and functionalization of TiO_2 nanoparticles, the color of the treated cotton changed from white to gray. The reflectance spectra of the cotton were consistent with the cotton color, which further demonstrated the successful deposition of the nano materials on the cotton [22]. The results depicted in Fig. 9 also shows that the functionalized textile substrates are not a composite but have separate and well adhered nanoparticle's coatings. When cotton were coated with one RGO coating (which is gray-colored), reflectance decreased due to the strong absorption of RGO in the visible region. It has been reported that the enhanced absorption of RGO in the visible region can also promote the transfer of excited electrons from RGO to the

conduction band of TiO_2 and then are transferred to the surface of TiO_2 where they react with oxygen to yield superoxide radicals that are able to oxidize organic compounds.

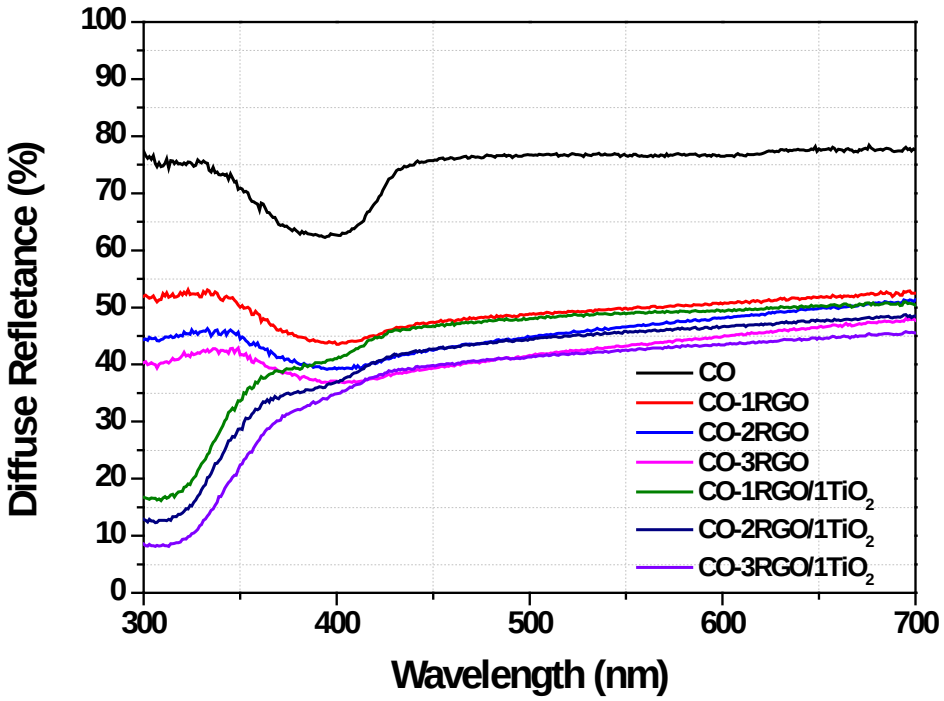

Fig. 8. Diffuse reflectance spectra for cotton (CO) and CO with RGO and RGO/TiO_2.

A correspondent measurement for light absorption can be defined through a parameter called the Kubelka–Munk function, F(R) [24]:

$$F(R) = (1 - R)^2/2R = \alpha/S, \quad (3)$$

where R, α and S are the reflectance, absorption and scattering coefficients, respectively. The absorption coefficient is related to the incident photon energy (E) by means of the Tauc's equation [21]:

$$\alpha = A\left(E - E_g\right)^m/E, \quad (4)$$

where A is a constant that depends on the properties of the material, Eg is the bandgap energy, and m is a constant that can take different values depending on the type of electron transition: for a direct allowed transition m =1/2 and for an indirect allowed transition m=2. This forbidden gap seems to be generated with an indirect allowed

transition, but as the direct forbidden transitions are weaker in strength, the indirect allowed transitions play a dominant role in the optical absorption [25]. Combining Eqs. 6 and 7, it is possible to plot the graph Fig 10 by which it is obtain the bandgap to indirect allowed transitions.

The energy bandgap of all samples remained around 3.2 eV, this value agrees with the bandgap of the indirect transition of anatase [25].

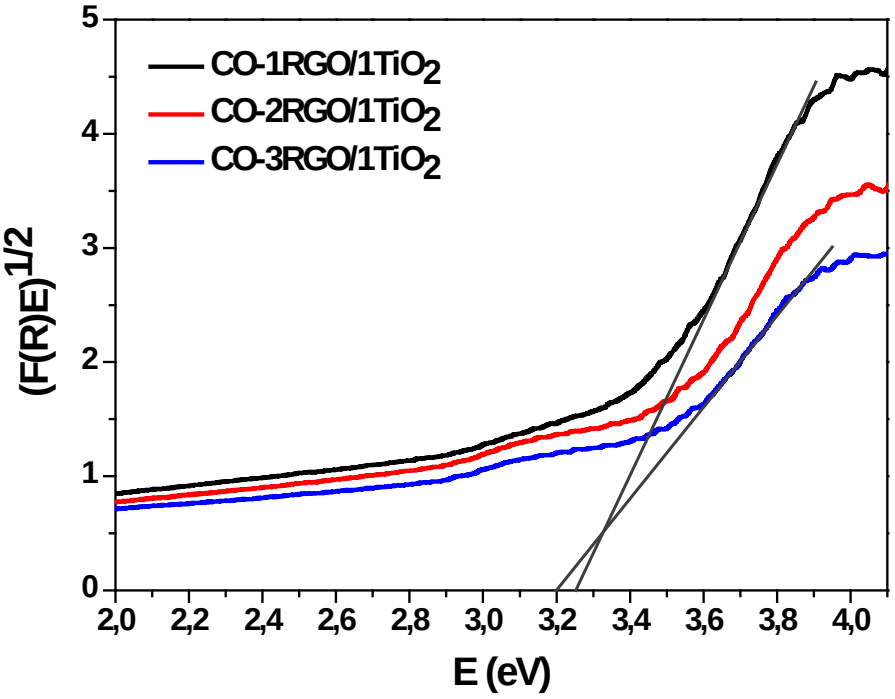

Fig. 9. Plot of Kubelka–Munk transform versus the energy of the light absorbed for CO-(1-3)RGO/1 TiO_2 before washing (B. W.) process, to indirect allowed transitions.

3.5 Electrochemical impedance spectroscopy (EIS) measurements

Impedance modulus vs. Frequency

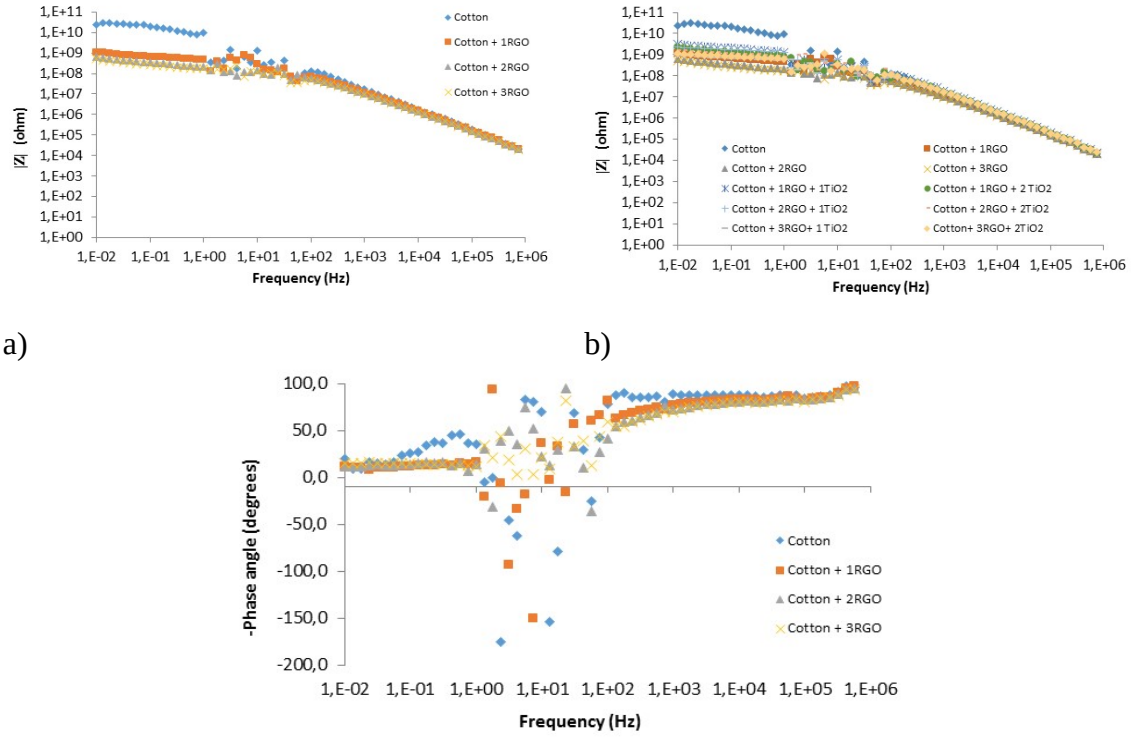

Fig. 10. **a) and b) Bode plots for cotton coated with different number of RGO coatings (1–3) and coated with different number of TiO2 nanoparticles (1-2). Measurements between two copper electrodes above the samples. Distance between electrodes 1.5cm. Cotton measured area 1.5cm × 1.5cm. c) Sample located between two metallic conductors. Frequency range for all the samples from 10^5Hz to 10^{-2}Hz.**

Slight decrease of the impedance modulus with the number of coatings. The TiO_2 is an insulating material, then dos not have influence on the conductivity. I would only include the first figure. Given the low conductivity, EIS in solution was not measured since significant results cannot be expected.

A lot of noise is observed in the central part due to the low conductivity of the materials. At high frequencies a –phase angle of around 90º is observed due to the low conductivity.

3.6 Electrochemical impedance spectroscopy (EIS) measurements in solution

3.7 Scanning electrochemical microscopy (SECM)

Negative feedback was observed for the PES-RGO-TiO2 samples showing the low conductivity of the samples.

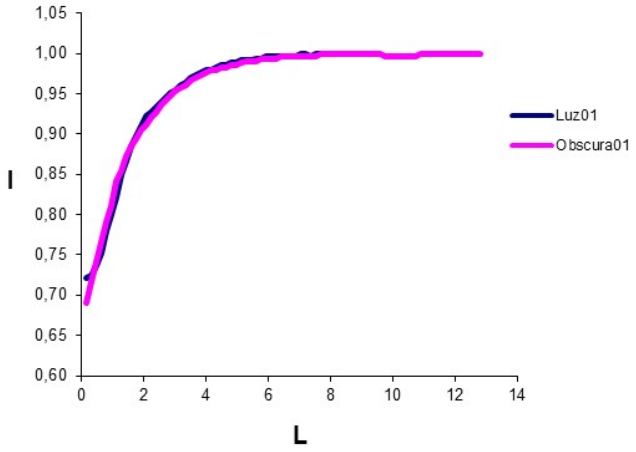

Fig. 11.

In the following experiment the current at the microelectrode tip was registered. It could be seen that under continuous illumination the current increased due to the generated photoelectrons. Under discontinuous illumination it could be seen that the sample was photo responsive. Light was turned at 60s till 180s. Turned again at 300 s till 420 s. When light was turned on, the current increased, when it was turned down, current decreased. Under no light, the current decreased.

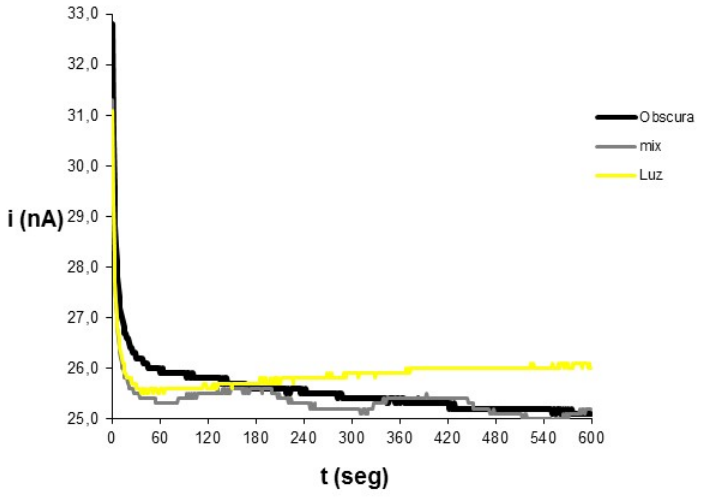

Fig. 12.

3.8 Photocatalytic activity before and after washing process

The photocatalytic activity of all samples was evaluated in terms of degradation of Rh-B under similar sunlight irradiation. Fig. 14 shows, for different irradiation times, the absorption spectra of Rh-B (4 mg/L) in the presence of sample CO-3RGO/1TiO_2. As can be observed, the maximum absorption peak, at around 554 nm, gradually decreases during the irradiation; the initial absorbance decreased about 87% after 120 min. The absorption maximum for all samples exhibited hypsochromic shifts, which suggests the stepwise formation of N-de-ethylated intermediates [26,27].

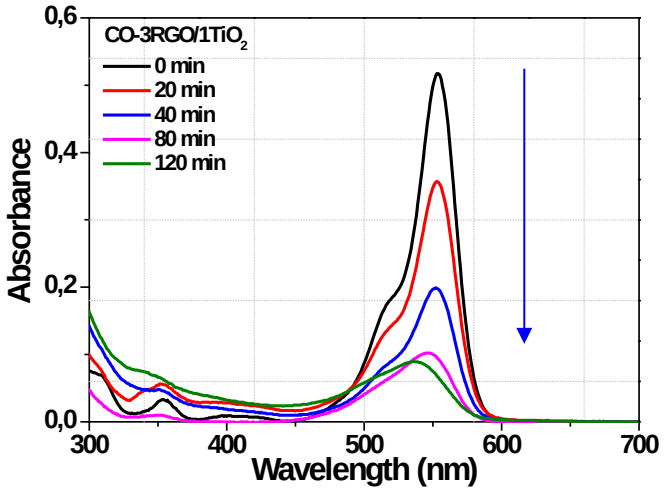

Fig. 14. Absorption spectra of Rh-B aqueous solution acquired at different irradiation times. The absorption data refer to the photocatalytic action of CO-3RGO/1TiO_2 placed in a laminar regime in a beaker with 400 mL of solution.

Fig. 15 shows the variation of the photocatalytic efficiency (η) of Rh-B aqueous solution degradation, that after 120 min: i) the increase of number of RGO coatings enhanced η (Eq. 2) in absence or presence of TiO_2 nanoparticle, ii) the samples CO-n_1RGO/n_2TiO_2 has better η than just CO-n_1RGO, iii) one or two coatings with TiO_2 has not changed significantly the η of samples functionalized with (1-3) RGO coatings, iv) even after the rigorous washing process (section 2.11) a high η remained.

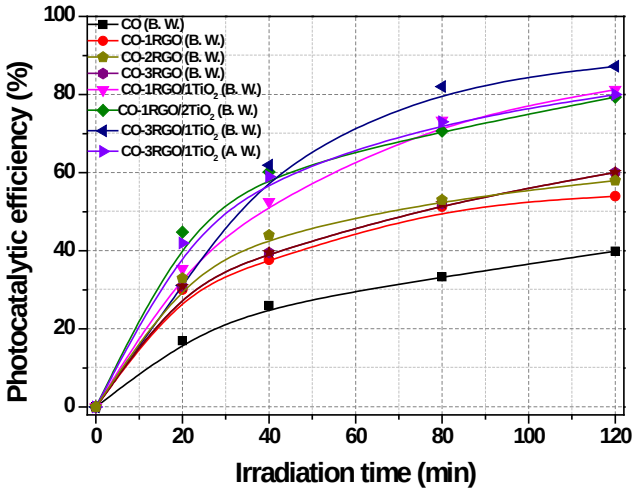

Fig. 15. Photocatalytic efficiency of CO, CO-(1-3)RGO, CO-1RGO/(1-2)TiO_2 before washing (B. W.) process and CO-3RGO/1TiO_2 before and after washing (A. W.) process.

As we know, one photon can usually induce the transfer of only one electron in photochemical reactions. Therefore, in the RGO/TiO_2 system, the RGO served as an electron collector and transporter to effectively separate the photogenerated electron–hole pairs created in TiO_2. This in turn lengthened the lifetime of the charge carriers, which could be advantageous for overcoming this obstacle to improve the degradation

of the Rh-B. During the photocatalytic reaction, a large number of electrons would be produced due to the highly dispersed TiO_2 nanoparticles over the RGO sheets (see Fig. 8). Furthermore, the large specific surface area of RGO also increased the adsorption of the dye molecules, thus favoring the photodegradation. Another mechanism (dye oxidation) of photocatalytic enhancement over the RGO/TiO_2 is depicted in Fig. 16.

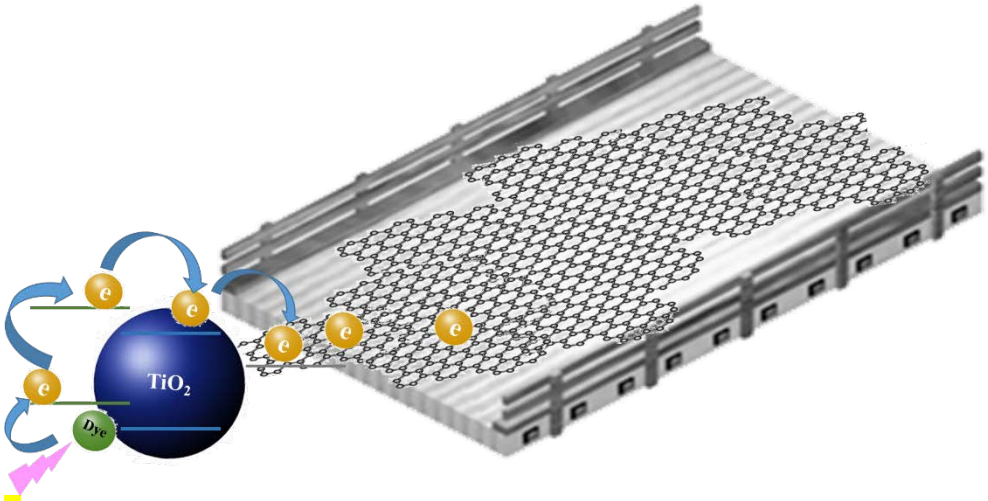

Fig. 16. Mechanism of photocatalytic enhancement over the RGO-TiO_2.

3.9 Morphological Analysis (SEM)

Fig. 8 shows micrographs of uncoated and functionalized cotton with RGO/TiO_2 coatings. Analysis from the SEM micrographs showed the cotton fiber surface is seen to be comprised of ridges. Higher magnification images of the cotton fiber surface indicates unevenness in these ridges where in some places the continuity of these structures is disturbed. The remaining samples which was coated with the lowest concentration of graphene oxide ($1gL^{-1}$) shows some deposition of graphene oxide on the fiber surface. A closer examination of the surface of the graphene oxide deposited fiber reveals a regular deposition of graphene oxide sheets. After graphene oxide reduction and functionalization by a mechanical process of nanoparticles of TiO_2 on cotton, the surfaces of the treated sample were completely coated by graphene and TiO_2

condensed to a coating. With the increase of the coating of TiO_2 nanoparticles in the graphene oxide reduced sheets dispersion becomes more prominent. The presence of titanium dioxide nanoparticles on the graphene sheets was confirmed. This reveals that graphene is densely decorated with titania nanoparticles. The average sizes of the TiO_2 nanoparticle are in the range of 20–30 nm, which is in good agreement with the size value estimated by XRD [8]. Additionally it is possible to verify in Fig.8 that after the washing process (5 washes 60° C) the adhesion of the nanoparticles to the cotton fiber remains high.

	Before Washing Process	**After Washing Process**	**EDS**
Cotton	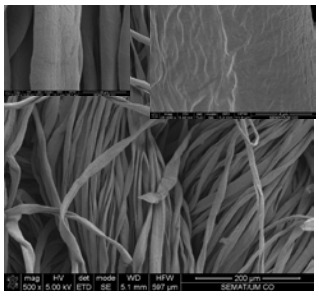	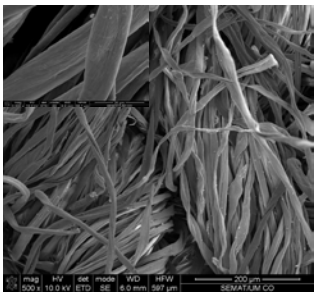	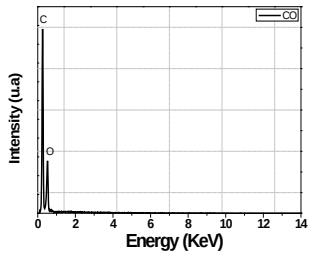
CO-1RGO	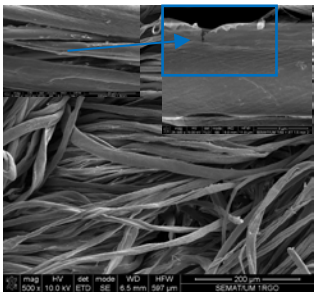	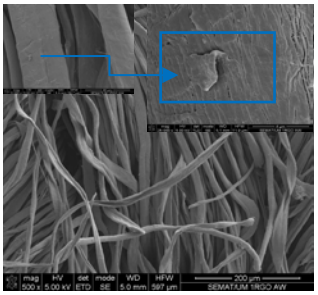	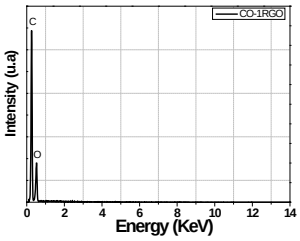
CO-3RGO	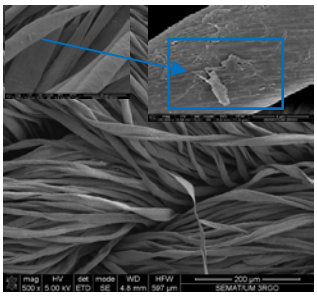	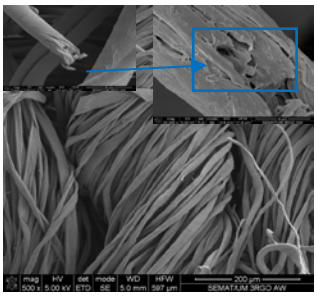	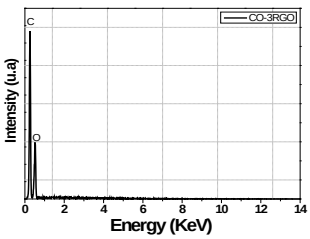

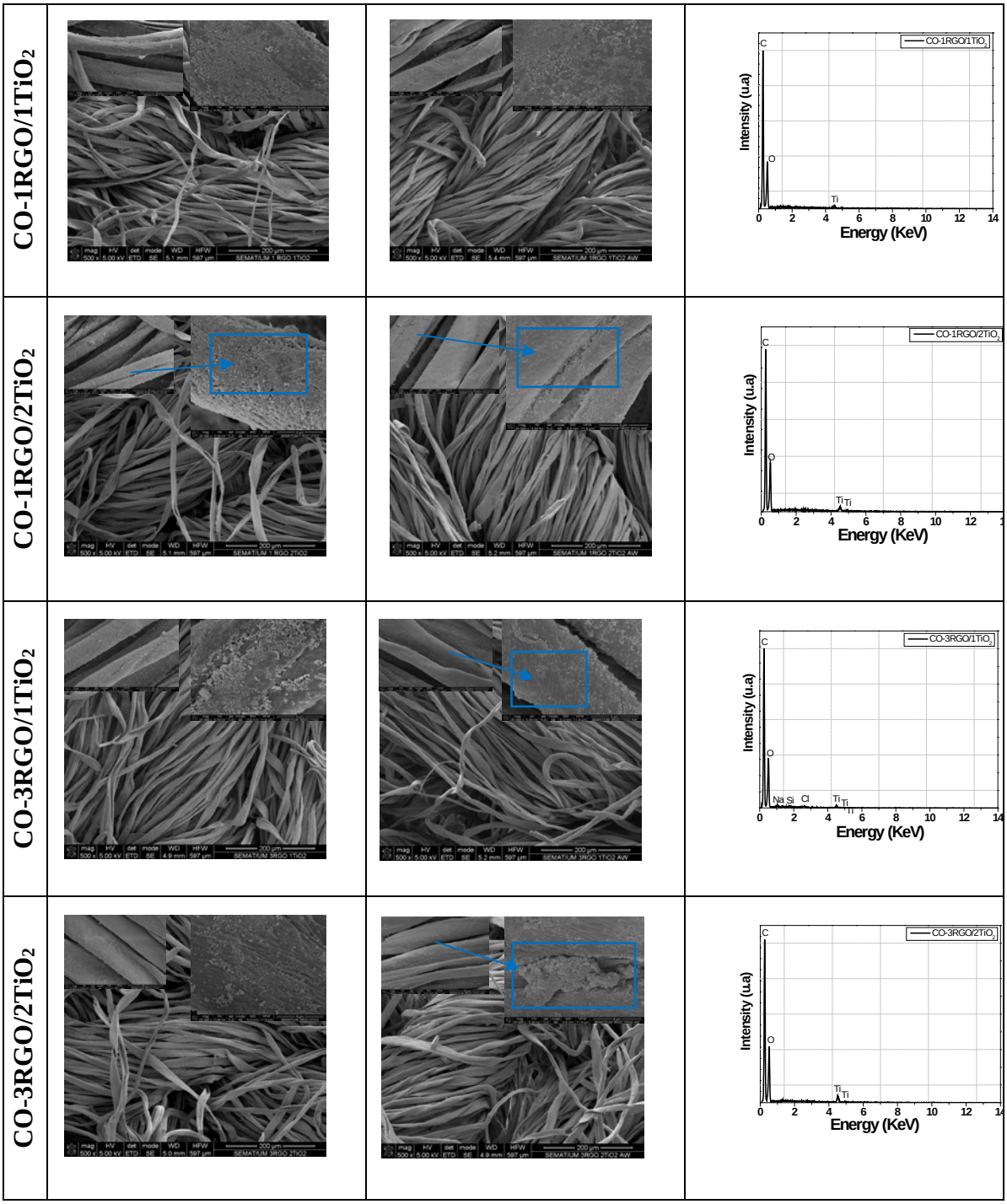

Fig. 13. Scanning electron microscope images of untreated cotton fiber surface and CO-1RGO/1TiO_2, CO-1RGO/2TiO_2, CO-3RGO/1TiO_2 and CO-3RGO/2TiO_2 samples, before and after washing process.

3.10 HPLC

HPLC chromatograms of the solution treated with CO-3RGO/1TiO_2 after 9 h under similar sunlight irradiation process were obtained using a UV-visible diode array detector and a mass detector (Fig. 17). The retention time of Rh-B in the conditions described above was 22.29 min. The five intermediates were observed, namely, DER (20.26 min), EER (17.86 min), DR (15.52 min), ER (12.54 min) and R (8.03 min), corresponding molecular masses of 415, 387, 387, 359 and 331, respectively. Once the ion peaks differed by 28 u in sequence, this is in agreement with the sequential loss of the ethyl groups from the Rh-B [26]. The evolution of the Rh-B concentration during the degradation process was determined using HPLC-MS and the concentration of this substrate at the end of the process corresponded to 2% of the initial value. The peak which appears at the beginning of the chromatograms indicate the presence of more polar compounds. The concentration of the identified products could not be determined considering the lack of appropriate standards.

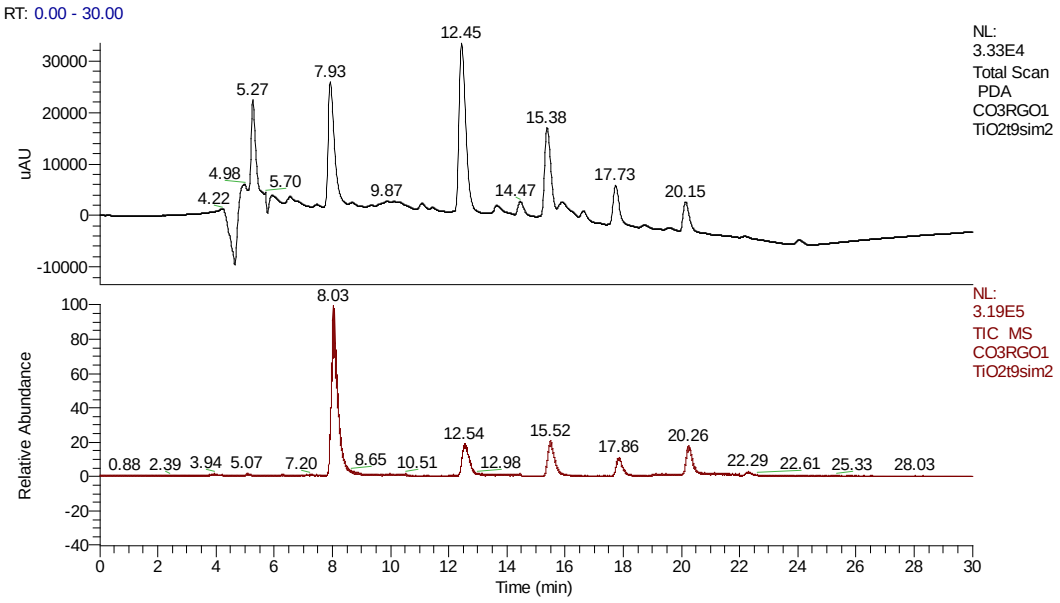

Fig. 17. Chromatograms corresponding to PDA (top) and MS detectors (bottom) respectively of the reaction mixture at the end of photocatalytic treatment with CO-3RGO/1TiO_2.

4. Conclusions

We have developed a novel method for deposition of TiO_2 nanoparticles on bleached cotton coated with reduced graphene oxide (RGO), and verified the method using zeta potential measurements. Different number of RGO (1-3) and TiO_2 (1-2) coatings were applied on cotton to study the influence of these parameters on the optical, electrical, electrochemical and photocatalytic properties. SEM and EDX results prove the presence of the RGO/TiO_2 coatings on the cotton before and after a rigorous a washing process, confirming a good adhesion of the TiO_2 nanoparticles on the cotton RGO coating. A high photocatalytic degradation efficiency (η) of Rh-B before and after the washing process also shows good adhesion of RGO/TiO_2 on the cotton.

An increase in the η of Rh-B (after 120 min) was observed with the increasing number of RGO layers, although the addition of TiO_2 to these samples CO-RGO further improved photocatalytic performance. This increase can be attributed to an electron transfer between TiO_2 nanoparticles and CO-RGO, which decreases the recombination of charge carriers generated in these materials.

Finally, the results of UV-vis (hypsochromic shifts) and HPLC/MS agreed for the presence of intermediates of degradation of Rh-B, although other products were not detected. Evidently, the cleavage of the ring structure of Rh-B molecule was not the principal reaction obtained in our experiments.

Acknowledgements

S. Landi Jr. expresses his gratitude to the Brazilian Coordenação de Aperfeiçoamento de Pessoal de Nível Superior (CAPES) for sporting his Doctoral Fellowship performed in Physics Centre at University of Minho. J. Molina wishes to thank the Spanish

Ministerio de Ciencia e Innovación (contract MAT2016-77742-C2-1-P) for the financial support. Moreover, the authors still want to thank the Portuguese Foundation for Science and Technology (FCT) for its contribution in financial support of this research work.

Reference

[1] U. I. Gaya and A. H. Abdullah, J. Photochem. Photobiol. C Photochem. Rev. **9**, 1 (2008).

[2] C. Chen, W. Ma, and J. Zhao, Chem. Soc. Rev. **39**, 4206 (2010).

[3] T. Janin, V. Goetz, S. Brosillon, and G. Plantard, Sol. Energy **87**, 127 (2013).

[4] L. Zang, **42**, 308 (2008).

[5] Y. He, N. B. Sutton, H. H. H. Rijnaarts, and A. A. M. Langenhoff, Appl. Catal. B Environ. **182**, 132 (2016).

[6] S. G. Kumar and L. G. Devi, J. Phys. Chem. A **115**, 13211 (2011).

[7] J. O. Carneiro, S. Azevedo, F. Fernandes, E. Freitas, M. Pereira, C. J. Tavares, S. Lanceros-Méndez, and V. Teixeira, J. Mater. Sci. **49**, 7476 (2014).

[8] J. Molina, F. Fernandes, J. Fernández, M. Pastor, a. Correia, a. P. Souto, J. O. Carneiro, V. Teixeira, and F. Cases, Mater. Sci. Eng. B **199**, 62 (2015).

[9] E. Pakdel and W. A. Daoud, J. Colloid Interface Sci. **401**, 1 (2013).

[10] B. Xu, J. Ding, L. Feng, Y. Ding, F. Ge, and Z. Cai, Surf. Coatings Technol. **262**, 70 (2015).

[11] C. T. Chang, J. J. Wang, T. Ouyang, Q. Zhang, and Y. H. Jing, Mater. Sci. Eng. B Solid-State Mater. Adv. Technol. **196**, 53 (2015).

[12] H. Zhang, X. Lv, Y. Li, Y. Wang, and J. Li, ACS Nano **4**, 380 (2010).

[13] Y. Gu, M. Xing, and J. Zhang, Appl. Surf. Sci. **319**, 2 (2014).

[14] K. Zhao, L. Feng, H. Lin, Y. Fu, B. Lin, W. Cui, S. Li, and J. Wei, Catal. Today **236**, 127 (2014).

[15] Y. Zhang and C. Pan, J. Mater. Sci. **46**, 2622 (2011).

[16] T. D. Nguyen-Phan, V. H. Pham, E. W. Shin, H. D. Pham, S. Kim, J. S. Chung,

E. J. Kim, and S. H. Hur, Chem. Eng. J. **170**, 226 (2011).

[17] Y. Haldorai, A. Rengaraj, C. H. Kwak, Y. S. Huh, and Y. K. Han, Synth. Met. **198**, 10 (2014).

[18] C. Nethravathi and M. Rajamathi, Carbon N. Y. **46**, 1994 (2008).

[19] S. Y. Toh, K. S. Loh, S. K. Kamarudin, and W. R. W. Daud, Chem. Eng. J. **251**, 422 (2014).

[20] S. Kashyap, S. Mishra, S. K. Behera, S. Kashyap, S. Mishra, and S. K. Behera, J. Nanoparticles, J. Nanoparticles **2014, 2014**, e640281 (2014).

[21] J. O. Carneiro, S. Azevedo, F. Fernandes, E. Freitas, M. Pereira, C. J. Tavares, S. Lanceros-Méndez, and V. Teixeira, J. Mater. Sci. **49**, 7476 (2014).

[22] L. Karimi, M. E. Yazdanshenas, R. Khajavi, A. Rashidi, and M. Mirjalili, Cellulose **21**, 3813 (2014).

[23] M. F. Abdel-Messih, M. a. Ahmed, and A. S. El-Sayed, J. Photochem. Photobiol. A Chem. **260**, 1 (2013).

[24] S. Valencia, J. M. Marin, and G. Restrepo, Open Mater. Sci. J. **4**, 9 (2010).

[25] A. F. Khan, M. Mehmood, S. K. Durrani, M. L. Ali, and N. a. Rahim, Mater. Sci. Semicond. Process. **29**, 161 (2014).

[26] C. Chen, W. Zhao, P. Lei, J. Zhao, and N. Serpone, Chem. - A Eur. J. **10**, 1956 (2004).

[27] T. Wu, G. Liu, J. Zhao, H. Hidaka, and N. Serpone, J. Phys. Chem. B **102**, 5845 (1998).